

PACS numbers: 42.65.Jx; 42.65.Re; 52.50.Jm
DOI: 10.1070/QE2009v039n07ABEH014049

Discrete conical emission rings observed upon filamentation of a femtosecond laser pulse in quartz

A.E. Dormidonov, V.P. Kandidov, V.O. Kompanets, S.V. Chekalin

Abstract. **Supercontinuum emission observed upon filamentation of transform-limited collimated femtosecond laser pulses in a transparent condensed medium (fused KU-1 quartz) is studied experimentally and numerically. The splitting of diverging conical supercontinuum emission into discrete rings was observed with increasing the pulse energy.**

Keywords: *filamentation, supercontinuum, conical emission, femtosecond pulse*.

1. Introduction

The superbroadening of high-power femtosecond pulses due to their self-action has long attracted the attention of researchers [1]. During filamentation of laser pulses in transparent dielectrics, the superbroadening of the frequency spectrum of a pulse occurs simultaneously with the broadening of its angular spectrum and formation of the so-called conical supercontinuum emission [2 – 4]. In media with the normal group velocity dispersion, the angular divergence of the conical supercontinuum emission increases with decreasing the wavelength λ of broadband radiation. As a result, along with the formation of an extended filament, a continuous rainbow-hued pattern of coloured rings is observed in the cross-sectional plane, the ring radius monotonically increasing with decreasing the supercontinuum emission wavelength.

Upon filamentation of emission in a medium with normal dispersion, the emission intensity distribution in variables θ, λ (θ is the divergence angle of conical emission in the medium) has the characteristic X-like shape, which is especially clearly observed in condensed media (for example, in water) for a pulse with the central wavelength lying in the visible range [5]. When the pulse is focused with an axicon, the continuous angular conical emission spectrum formed upon pulse filamentation in a K108 glass is decomposed into narrow rings separated by interference minima [6]. The appearance of angle-discrete conical emission rings upon filamentation of a phase-modulated pulse in air was discussed in [7]. The decomposition of the angle-continuous conical emission spectrum into discrete rings upon filamentation of a 800-nm pulse in fused silica was reported in [8]. Discrete conical emission rings were observed in [9] upon filamentation of a femtosecond laser pulse in a BaF_2 crystal.

In this paper, we studied supercontinuum conical emission observed upon filamentation of a collimated femtosecond laser pulse in fused silica. The formation of supercontinuum conical emission during filamentation of pulses of different energies was analysed experimentally and numerically. A simple interference model was proposed to interpret the experimental results obtained in the study.

2. Experimental setup

Supercontinuum conical emission was studied by using a femtosecond spectroscopic stand built at the Collective usage centre at the Institute of Spectroscopy, RAS (Troitsk). The stand can be used to measure the frequency-angular supercontinuum intensity distribution upon filamentation of 800-nm femtosecond pulses of energy up to 1 mJ in condensed media and of energy up to 100 μJ with the use of a parametric amplifier allowing wavelength tuning in a broad spectral range (Fig. 1). The setup consists of a tunable TOPAS parametric amplifier combined with a regenerative Spitfire Ti : sapphire amplifier. Pulses from a femtosecond Tsunami Ti : sapphire laser pumped by a cw Millenia Vs solid-state laser are supplied to the regenerative amplifier. The regenerative amplifier is pumped by a pulsed Evolutiion X solid-state laser (all the instruments are manufactured by Spectra-Physics). The parametric TOPAS amplifier emits femtosecond pulses of duration from 35 to 150 fs in the spectral range from 250 to 10000 nm (depending on a converter used).

Experiments were performed by using 800-nm, 35-fs pulses with a pulse repetition rate of 1 kHz. The spectral full width at half-maximum (FWHM) of pulses was ~ 20 nm. Pulse parameters were controlled with a power meter and an autocorrelator measuring the autocorrelation function in the range from 460 to 1100 nm. The output beam diameter of the laser setup was 3 mm (FWHM).

Conical emission was produced by focusing femtosecond radiation by a lens with a focal length of 100 cm on a sample. The position and diameter of the beam waist, in which the input end of a KU-1 fused silica sample was placed, were determined with an LBP-2 profilometer. Thus, a sample of size $3 \times 3 \times 13.5$ cm was irradiated by transform-limited collimated laser pulses. The laser beam

A.E. Dormidonov, V.P. Kandidov Department of Physics, M.V. Lomonosov Moscow State University, Vorob'evy gory, 119991 Moscow, Russia; e-mail: kandidov@phys.msu.ru;
V.O. Kompanets, S.V. Chekalin Institute for Spectroscopy, Russian Academy of Sciences, 142190 Troitsk, Moscow region, Russia; e-mail: kompanetsvo@isan.troitsk.ru, chekalin@isan.troitsk.ru

Received 20 January 2009
Kvantovaya Elektronika **39** (7) 653 – 657 (2009)
Translated by M.N. Sapozhnikov

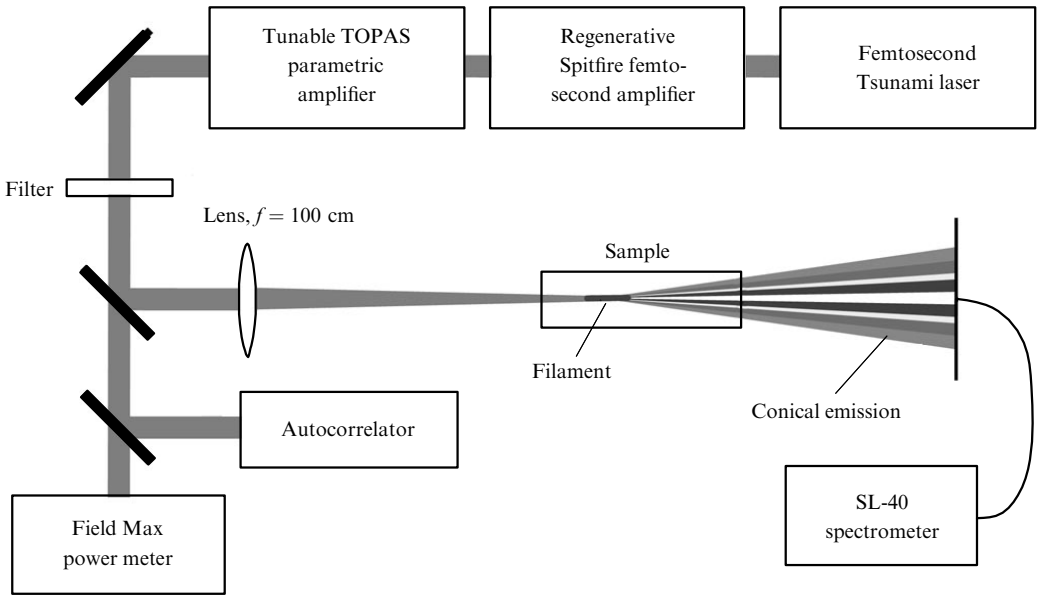

Figure 1. Scheme of the spectroscopic stand for measuring the frequency-angular distribution of supercontinuum emission upon filamentation of a femtosecond laser pulse in condensed media.

diameter on the input end was 100 μm. A constant radiation power level was maintained during measurements with the help of a neutral variable-density (0–2 OD) disc filter of diameter 10 cm. The formation of luminous filaments with a high energy density and, hence, the ionisation regions of matter (plasma channels) was recorded with a mirror digital Canon EOS 400D camera through the side face of the sample. By recording emission produced due to the recombination of the filament laser plasma, we determined the length and position of plasma channels and estimated the electron concentration in them from the filament emission brightness.

The supercontinuum conical emission was observed on a white screen placed at a distance of 20 cm from the output face of the sample. The conical emission pattern observed on the screen was recorded with the digital Canon EOS 400D camera, which provided the required spatial resolution and the colour reproduction of the image. The frequency-angular intensity distribution was measured with a fibre spectrometer with the measurement head moved in the cross section of the conical emission pattern.

3. Experimental results

Supercontinuum conical emission and filaments in a sample were recorded by changing the pulse energy from 0.5 to 10 μJ. When the pulse energy exceeded 0.8 μJ, a red spot appeared at the screen centre, which became yellow-green with increasing the pulse energy up to 1.1 μJ, and then white (1.3 μJ), which demonstrates the continuous broadening of the supercontinuum spectrum. At pulse energies in the range from 1.3 to 1.8 μJ, coloured conical emission rings appeared around the white spot. The radius of these rings increased monotonically with increasing the anti-Stokes frequency shift. The divergence angle for the short-wavelength region of the conical emission spectrum was ~ 0.1 rad. At a distance of 12 mm from the input face inside a sample, a plasma channel of length 2–3 mm was formed (Fig. 2a). As the pulse energy was increased up to 1.9 μJ and above, the angle-continuous spectrum of concentric conical emission rings decomposed into a number of discrete narrow coloured rings separated by low-intensity dark rings (Figs 2b, c). In this case, the dependence of the radius of coloured rings on their wavelength, which is typical of conical emission, preserved. The angular width of coloured rings equal to ~ 0.01 rad was comparable with the width of temperature rings.

The type of a filament inside the sample changed qualitatively with increasing laser pulse energy. Thus, after

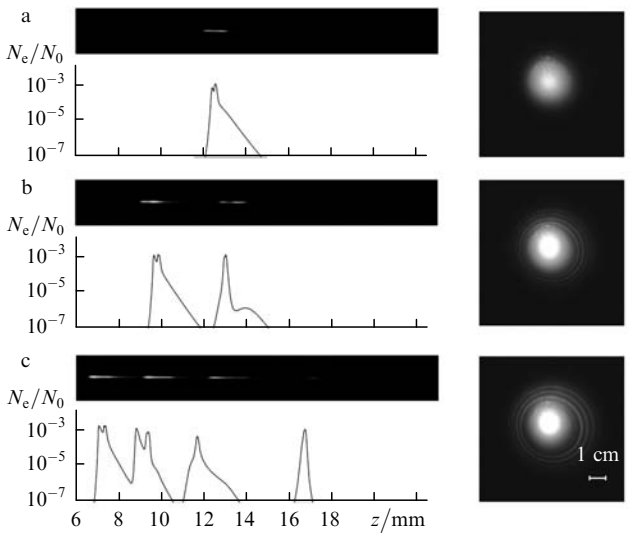

Figure 2. Splitting of conical emission rings in a fused silica sample during filamentation of 800-nm, 35-fs pulses. At the left: photographs of the images of plasma channels taken with a camera through the side face of the sample; the curves are the electron concentrations $N_e(z)$ at the axis of plasma channels calculated numerically; at the right: images of conical emission taken with a camera. The pulse energies are 1.3 (a), 1.9 (b), and 2.4 μJ (c).

the formation of the first plasma channel at a distance of 9 mm from the input end of the sample at the pulse energy of 2 μJ, the second plasma channel appeared on the filament axis at some distance from the first filament (Fig. 2b). The total length of the plasma channel and, hence, of the source of the broadband supercontinuum emission increased up to 5–6 mm. Pulses with energy of 2.4 μJ formed a successive chain of four plasma channels of the total length exceeding 8 mm. As the laser pulse energy was increased, the rings became brighter, their angular width increasing.

Pulses of energy exceeding 5 μJ give rise to numerous filaments and related plasma channels randomly located in the beam cross section. The superposition of conical emission from these numerous coherent sources leads to the 'blurring' of discrete emission rings and formation of a speckle pattern, which is irregular from pulse to pulse in the general case [6].

4. Numerical simulation

Conical emission was analysed theoretically by using a model of filamentation of femtosecond laser pulses in condensed media and the software developed for numerical simulations of supercontinuum generation during the filamentation of radiation in a broad wavelength range. The model describes the diffraction and nonlinear-optical interaction of femtosecond radiation with a medium taking into account the material dispersion in the condensed medium according to the Sellmeyer formula. The equation for the slowly varying pulse amplitude was obtained by retaining the terms of the second-order smallness in time derivatives [10]. This allows us to reproduce the wave nonstationarity during pulse self-modulation, which is manifested in the increase in the slope of the trailing edge of the pulse and formation of the envelope shock wave [1]. As a result, the frequency range reproduced in the slowly varying amplitude method is considerable extended, which is required for the correct description of the pulse superbroadening upon self-action.

By simulating numerically the filamentation of femtosecond laser pulses under our experimental conditions, we obtained the distributions $N_e(r, z)$ of free electrons in plasma channels and of the complex envelope $E(r, t)$ of the light field for pulses at the carrier frequency ω_0. Figure 2 presents the calculated free electron concentrations $N_e(z)$ on the axis of plasma channels formed by pulses with energies 1.3, 1.9, and 2.4 μJ. As the pulse energy was increased, a chain of successive plasma channels appeared in the silica volume. The chain of plasma channels is produced due to multiple refocusing of a laser pulse in a nonlinear medium. Note that the material dispersion of the medium strongly affects refocusing during pulse filamentation. As shown in [11], in a medium with a strong material dispersion, multiple refocusing appears in a pulse with the peak power exceeding the critical self-focusing power by hundreds of times. The geometrical parameters of plasma channels, their length and location in the medium coincide with the experimental data. The peak electron concentration $N_e(r, z)$ calculated numerically changes nonmonotonically along individual plasma channels. Thus, the concentration profile $N_e(z)$ (Fig. 2a) contains two pronounced maxima, which completely corresponds to the 'dumbbell-like' image of plasma regions observed in experiments. Analysis of the results of numerical simulation showed that such an inhomogeneity of the plasma channel is caused by the formation of the secondary maximum on the pulse profile due to the refocusing of its tail part in the case of a strong material dispersion.

The frequency-angular spectrum of a laser pulse is described by the expression

$$S(k_\perp, \Omega) = \text{const}\left| \int_0^\infty \int_{-\infty}^\infty E(r, t) J_0(k_\perp r) \mathrm{e}^{-\mathrm{i}\Omega t} r \mathrm{d}r \mathrm{d}t \right|^2, \quad (1)$$

where $J_0(k_\perp r)$ is the zero-order Bessel function; $\Omega = \omega - \omega_0$ is the frequency shift of supercontinuum emission at the frequency ω from the carrier frequency ω_0; $k_\perp = \sqrt{k^2 - k_z^2}$ is the transverse component of the wave vector $k(\omega) = \omega n(\omega) c^{-1}$; and $n(\omega)$ is the refractive index of the medium. To compare the spectral intensity with experimental data, we made the change of variables from $k_\perp, \Omega$ to θ, λ (where $\theta = k_\perp/k$, $\lambda = 2\pi c/\omega$). It follows from the energy relation

$$E = \int\int S(k_\perp, \omega = \omega_0 + \Omega) \mathrm{d}k_\perp \mathrm{d}\omega = \int\int S(\theta, \lambda) \mathrm{d}\theta \mathrm{d}\lambda \quad (2)$$

that [12]

$$S(\theta, \lambda) = S(k_\perp, \omega) \frac{n(\omega)\omega^3}{2\pi c^2}. \quad (3)$$

Taking into account the spectral sensitivity $h(\lambda)$ of a digital camera used to record the distribution of conical emission on the screen, we obtained the angular distribution of the spectral emission components in the laboratory experiment format:

$$S_h(\theta, \lambda) = S(\theta, \lambda) h(\lambda). \quad (4)$$

The spectral sensitivity $h(\lambda)$ is close to the human eye sensitivity and has a maximum in the green spectral region, strongly falling at the boundaries of the visible range. The spectrum $S_h(\theta, \lambda)$ can be called 'visible' because it corresponds to the broadband emission spectrum of perceptible to the eye.

Figure 3 presents at the logarithmic scale the tone images of 'visible' frequency-angular spectra $S_h(\theta, \lambda)$ of laser pulses with energies 1.3, 1.9 and 2.4 μJ calculated for our experimental conditions. One can see that the regions of the maximum intensity of spectral components $S_h(\theta, \lambda)$ in the (θ, λ) plane are shifted to modulo greater angles θ with decreasing the supercontinuum wavelength, thereby forming diverging conical emission. When the pulse energy is low (Fig. 3a), the angle θ increases monotonically with decreasing λ, which corresponds to the formation of continuous conical emission rings in the far-field zone, which are observed in experiments (Fig. 2a). As the pulse energy is increased up to 1.9 and 2.4 μJ (Figs 3b, c), the frequency-angular distribution $S_h(\theta, \lambda)$ becomes modulated both over the divergence angle and the wavelength. The angular modulation, which is especially pronounced in the vicinity of a wavelength of 650 nm, reproduces the splitting of conical emission into discrete red rings observed in experiments (Figs 2b, c). In this case, the angular width of discrete rings in the spectrum $S_h(\theta, \lambda)$ increases with increasing pulse energy.

The numerical and experimental results are compared in Fig. 4, where the angular dependences of the spectral

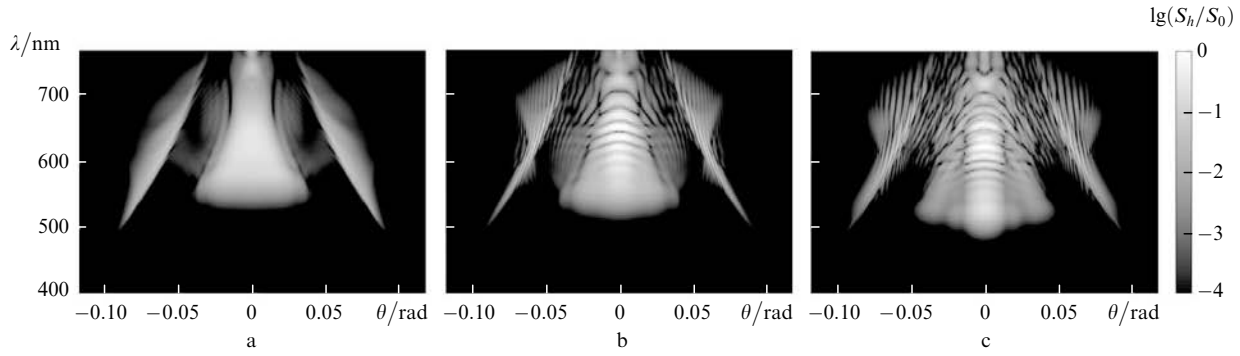

Figure 3. Tone images of the 'visible' frequency-angular spectra $S_h(\theta, \lambda)$ of laser pulses during filamentation in fused silica calculated numerically for experimental conditions at pulse energies 1.3 (a), 1.9 (b) and 2.4 μJ (c); S_0 is the normalisation factor.

components $S_h^{\Delta\lambda}(\theta) = \int_{\lambda_1}^{\lambda_2} S_h(\theta, \lambda)\mathrm{d}\lambda$ calculated for a number of wavelength intervals $\lambda_1 - \lambda_2$ in the visible spectral region are presented. When the pulse energy is low (1.3 μJ), one side maximum exists in each separated wavelength interval (Fig. 4a), which corresponds to continuous rainbow conical emission rings (Fig. 2a). Thus, for $\theta = 0.08$ rad, the green line maximum exists in the region 480 – 560 nm, which corresponds to the external green ring observed in experiments. For the pulse energy of 2.4 μJ (Fig. 4b), the angular distribution of the red spectral component (600 – 730 nm) contains several pronounced side maxima corresponding to the red discrete conical emission rings.

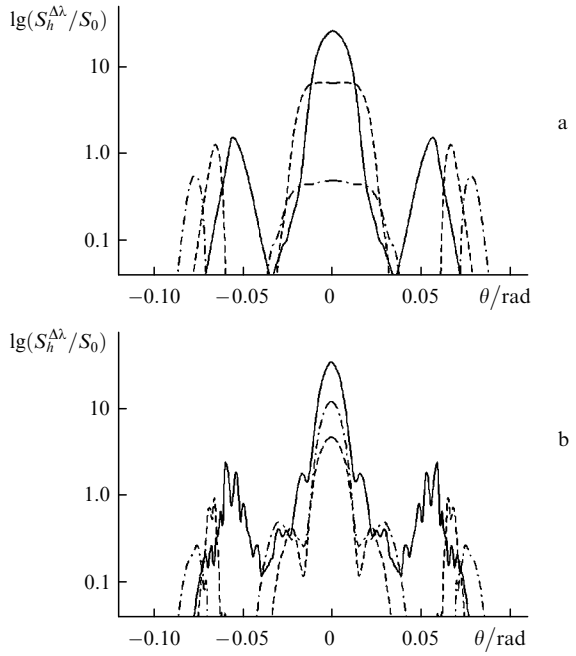

Figure 4. Angular dependences of the spectral components $S_h^{\Delta\lambda}(\theta)/S_0$ calculated for the red (600 – 730 nm, solid curve), yellow (580 – 600 nm, dashed curve), and green (480 – 560 nm, dot-and-dash curve) wavelength regions for pulse energies 1.3 (a) and 2.4 μJ (b).

5. Interpretation of the results

The appearance of modulation of the spectral intensity with increasing laser pulse energy can be explained by using a simple interference model. According to [1, 4], the frequency-angular superbroadening of the pulse spectrum upon filamentation appears due to the self-phase modulation of emission caused by the medium nonlinearity and induced laser plasma, the supercontinuum sources in a filament being coherent. This conclusion was confirmed experimentally in [13], where it was shown that the coherence of the supercontinuum is not worse than that of the initial pulse. Consider, for example, the case of formation of conical emission when two plasma channels are produced in the fused silica volume, which corresponds to the energy 1.9 μJ (Fig. 2b). We assume that conical emission is the result of interference of diverging broadband emission from two coherent sources separated by a distance l. Let us also assume that the frequency-angular emission spectrum of each source coincides with the spectrum $S(\theta, \lambda)$ of a 1.3-μJ pulse at which one plasma channel is formed (Fig. 3a). The phase difference between the waves at the wavelength λ emitted by these sources at an angle of θ is (Fig. 5)

$$\Delta\varphi(\theta, \lambda) = l\left\{\frac{\omega_0 - \omega}{v_g} - [k_0 - k(\omega)\cos\theta]\right\}$$

$$= \frac{2\pi l}{\lambda_0}\left\{\left(1 - \frac{\lambda_0}{\lambda}\right)\frac{c}{v_g} - \left[1 - \frac{\lambda_0 n(\lambda)}{\lambda n(\lambda_0)}\cos\theta\right]n(\lambda_0)\right\}. \quad (5)$$

Here, we take into account that he second source is formed by fundamental radiation at the wavelength $\lambda_0 = 2\pi c/\omega_0$ at a distance of l from the first source. It can be easily shown that the far-field spectral intensity of the total broadband radiation from two sources is described by the expression

$$S^{\Sigma}(\theta, \lambda) = 4S(\theta, \lambda)\cos^2(\Delta\varphi(\theta, \lambda)/2). \quad (6)$$

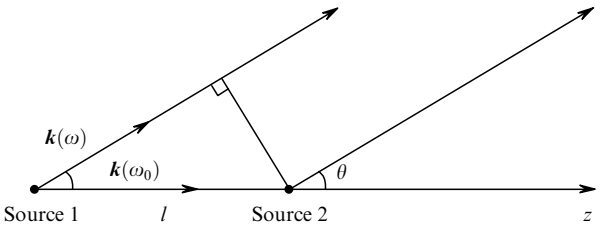

Figure 5. To the calculation of the phase difference between plane waves emitted by coherent sources separated by a distance of l.

Figure 6 presents the tone image of the frequency-angular spectrum $S_h^{\Sigma}(\theta, \lambda)$ calculated for a source with the 'visible' emission spectrum $S_h(\theta, \lambda)$ (Fig. 3a) by expression (6) for $l = 2.5$ mm. One can see that the modulation of the spectral intensity over the angle θ and wavelength λ coincides with that obtained by numerical simulation (Fig. 3b). This suggests that the angular splitting of conical emission rings occurs due to the interference of radiation from a sequence of extended coherent sources produced during multiple refocusing of the laser pulse in a medium with a strong material dispersion.

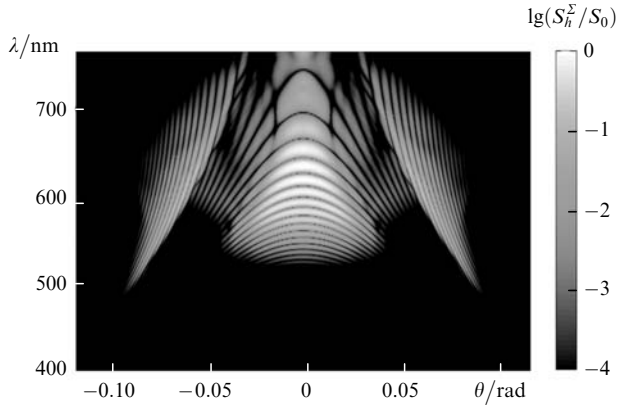

Figure 6. Tone image of the frequency-angular emission spectrum $S_h^{\Sigma}(\theta, \lambda)$ appearing due to the interference of conical emission from two coherent sources separated by a distance of 2.5 mm with unmodulated spectra $S_h(\theta, \lambda)$ (Fig. 3a).

6. Conclusions

We have found experimentally and studied theoretically for the first time the formation of many discrete rings from the angle-continuous conical emission spectrum upon filamentation of a transform-limited collimated femtosecond laser pulse in fused silica. The numerical simulation of filamentation of pulses of different energies has shown that the angular splitting of conical emission rings occurs due to the interference of emission from several extended coherent sources which are formed during multiple refocusing of a pulse in a medium with a strong material dispersion.

Acknowledgements. This work was supported by the Russian Foundation for Basic Research (Grant No. 08-02-00517-a).

References

1. Akhmanov S.A., Vysloukh V.A., Chirkin A.S. *Optika femtosekundnykh lazernykh impul'sov* (Optics of Femtosecond Laser Pulses) (Moscow: Nauka, 1988).
2. Nibbering E.T.J., Gurley P.F., Grillon G., Prade B.S., Franco M.A., Salif A., Mysyrowicz A. *Opt. Lett.*, **21**, 62 (1996).
3. Kosareva O.G., Kandidov V.P., Brodeur A., Chien C.Y., Chin S.L. *Opt. Lett.*, **22**, 1332 (1997).
4. Kandidov V.P., Kosareva O.G., Golubtsov I.S., Liu W., Becker A., Akozbek N., Bowden C.M., Chin S.L. *Appl. Phys. B*, **77**, 149 (2003).
5. Couairon A., Gaižauskas E., Faccio D., Dubietis A., Di Trapani P. *Phys. Rev. E*, **73**, 016608 (2006).
6. Kompanets V.O., Chekalin S.V., Kosareva O.G., Grogor'evskii A.V., Kandivdov V.P. *Kvantovaya Elektron.*, **36**, 821 (2006) [*Quantum Electron.*, **36**, 821 (2006)].
7. Chin S.L., Hosseini S.A., Liu W., Luo Q., Theberge F., Akozbek N., Becker A., Kandidov V.P., Kosareva O.G., Schroeder H. *Canad. J. Phys.*, **83**, 863 (2005).
8. Dormidonov A.E., Kandidov V.P., Kosareva O.G., Kompanets V.O., Chekalin S.V. *Proc. 2nd Int. Symp. Filamentation* (Paris, 2008) p. 87.
9. Dharmadhikari A.K., Dharmadhikari J.A., Mathur D. *Appl. Phys. B*, **94**, 259 (2009).
10. Brabec T., Krausz F. *Phys. Rev. Lett.*, **78**, 3282 (1997).
11. Liu W., Chin S.L., Kosareva O.G., Golubtsov I.S., Kandidov V.P. *Opt. Commun.*, **225**, 193 (2003).
12. Faccio D., Couairon A., Di Trapani P. *Conical Waves, Filaments and Nonlinear Filamentation Optics* (Roma: Aracne, 2007).
13. Chin S.L., Brodeur A., Petit S., Kosareva O.G., Kandidov V.P. *J. Nonlinear Opt. Physics Mat.*, **8,** 121 (1999).